ACS APPLIED NANO MATERIALS

www.acsanm.org Article

Stable Semi-Hollow Gold-Silver Nanostars with Tunable Plasmonic Resonances Ranging from Ultraviolet–Visible to Near-Infrared Wavelengths: Implications for Photocatalysis, Biosensing, and Theranostics

Nhat M. Ngo, Mina Omidiyan, Hung-Vu Tran, and T. Randall Lee*

Cite This: *ACS Appl. Nano Mater.* 2022, 5, 11391–11399 Read Online

ACCESS | Metrics & More | Article Recommendations | Supporting Information

ABSTRACT: This paper reports the fabrication of highly stable semi-hollow gold-silver nanostars (hAuAgNSts). Galvanic replacement between silver nanostars (AgNSts) and chloroauric acid afforded optically tunable hAuAgNSts with plasmonic resonances ranging from UV to visible to near-infrared wavelengths. Moreover, the compositionally unique bimetallic hAuAgNSts exhibited strong extinction maxima in the UV–vis range, which contrasts AgNSts (centered in the UV) and the more common gold nanostars (AuNSts; centered largely in the near infrared). Notably, the hAuAgNSts exhibited enhanced thermal and colloidal stability without the need for surface modification when compared to AgNSts and AuNSts. This latter feature offers additional opportunities in the fields of photocatalysis and photovoltaics as well as alternative strategies for post-synthetic modification that enable applications in biosensing and theranostics.

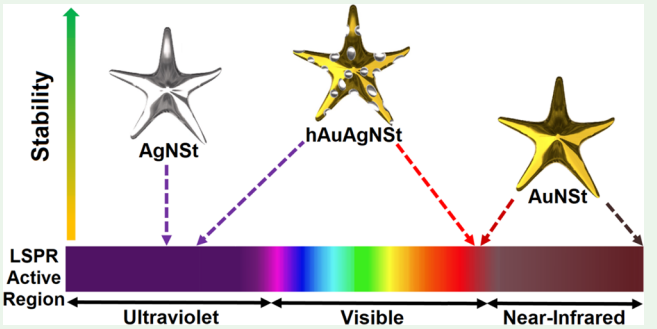

KEYWORDS: *nanostars, gold, silver, nanoparticle, plasmonic, bimetallic, semi-hollow, biomedical, stability*

INTRODUCTION

Metallic nanostructures have been studied for years because of their unique plasmonic properties and potential applications in various fields including solar cells, energy storage, sensing and biosensing, and biomedical applications including treatments for COVID-19 infection.[1−9] Under the illumination of an electromagnetic field, noble metal nanostructures exhibit localized surface plasmon resonance (LSPR) that arises from the collective oscillation of the delocalized electron cloud induced by an incident electromagnetic field.[10] This localized resonance phenomenon leads to numerous exotic properties of plasmonic nanostructures such as optical absorption,[11] spectroscopic enhancement,[12] plasmonic heating,[13] hot electron injection,[14] and plasmon-induced resonance energy transfer.[15]

Metallic nanostars such as gold nanostars (AuNSts) and silver nanostars (AgNSts) represent a relatively new class of plasmonic nanostructures with unique and attractive optical characteristics.[16−18] The morphologies of these nanostars provide enhanced surface-to-volume ratios compared to more conventional plasmonic nanostructures (e.g., nanospheres and nanorods). With many interfacial spikes, plasmonic nanostars[19] can produce intense electromagnetic fields with numerous electromagnetic hotspots compared to other structures[20] including nanospheres,[21] nanotripods,[22] nanocubes,[21] nanotriangles,[23] and nanorods.[24]

Although AuNSts offer greatly enhanced properties compared to conventional plasmonic nanostructures due to their unique shape, control of the optical properties of AuNSts requires delicate handling of the synthetic steps to obtain reproducible sizes and morphologies.[25,26] Further, due to their modest stability, gold nanostars usually require judicious surface modification, which can limit their use in certain applications. Importantly, their greatly intensified electromagnetic fields, their superior surface-to-volume ratios, and their inherent biocompatibility have enabled unique opportunities for a wide range of applications[20] including optoelectronics,[16] biosensing,[27,28] catalysis,[29,30] photovoltaics,[31,32] spectroscopies,[33,34] light-controlled therapies,[35] and drug delivery.[36] Strategies to overcome the synthetic challenges[25,37] include growing a secondary nanostructure[34] or creating core–shell structures[38] to tune the plasmonic

Received: June 6, 2022
Accepted: July 18, 2022
Published: August 11, 2022

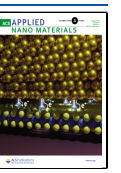

Scheme 1. Synthesis of Silver Nanostars and Semi-Hollow Gold-Silver Nanostars

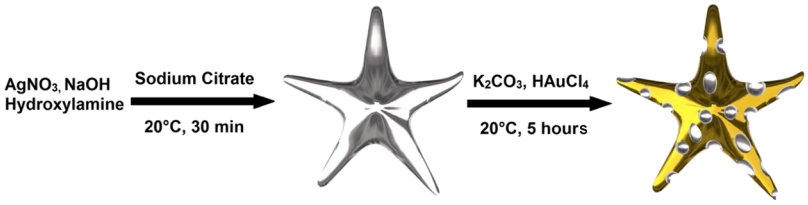

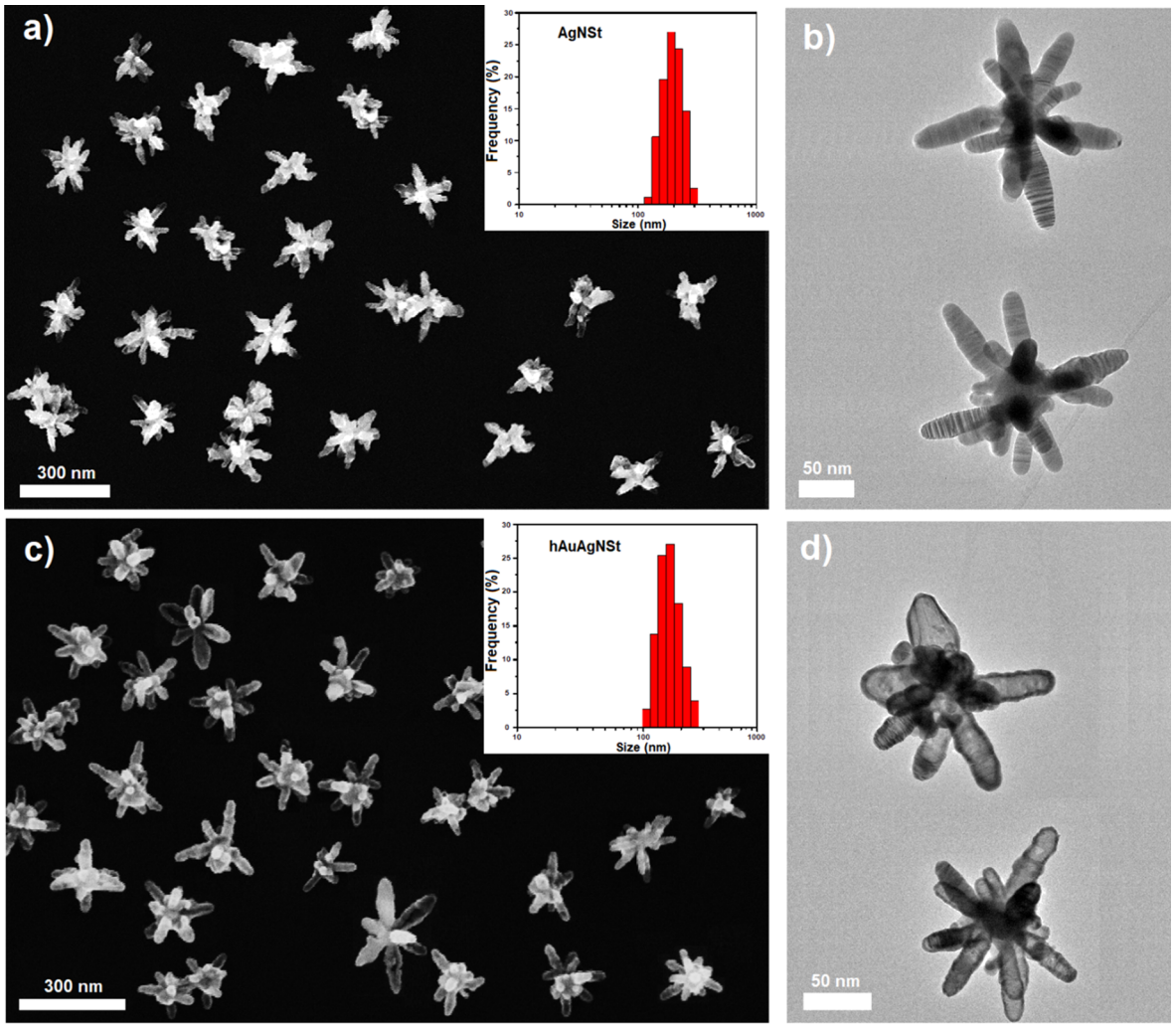

Figure 1. (a) SEM, (b) TEM images, and size distribution (inset) of the silver nanostar (AgNSt) starting materials and (c) SEM, (d) TEM images, and size distribution (inset) of the semi-hollow gold-silver nanostars (hAuAgNSts).

properties of the nanostars. However, these approaches require even more careful handling and modification to obtain the desired optical properties. Moreover, the optical range of these nanostructures is confined to ~700 nm to near-infrared (NIR) wavelengths,[29,39] which further limits their breadth of applications.

Another bottleneck in the development and applications of AuNSts is their propensity for aggregation, which occurs for many types of gold nanostructures.[40−42] The common strategy employed to deal with this problem is to functionalize the Au nanostructures with stabilizing ligands.[43−45] This additional modification step, however, further complicates the synthetic process; moreover, the introduction of a molecular coating layer can negatively impact applications that require intimate contact between the electromagnetic field of the metallic nanostars, such as catalysis or photovoltaics.[46−48]

Silver nanostars (AgNSts) have also been used in several applications, such as surface-enhanced Raman spectroscopy (SERS)-based sensing[49−52] and antimicrobial surfaces.[53] Notably, the plasmonic resonance wavelengths of silver nanostars (~375 nm)[49] are found in the ultraviolet region in contrast to the usual range for gold nanostars (~700 nm and longer).[29,39] However, the LSPR peak position of silver nanostars exhibits limited tunability, remaining largely constant despite changes in particle size,[54] which limits the practical applications of AgNSts in solar-powered applications such as photocatalysis and photovoltaics because the ability to operate in the visible region (400−700 nm), which makes up ~43% of

https://doi.org/10.1021/acsanm.2c02462
ACS Appl. Nano Mater. 2022, 5, 11391−11399

solar energy that reaches the surface of the earth,[55] is critical for optimal performance.

In this work, we report the synthesis and characterization of a new nanostar architecture: semi-hollow gold-silver nanostars (hAuAgNSts), which we prepared via galvanic replacement on AgNSts, as shown in Scheme 1. The new bimetallic gold-silver nanostars were characterized by electron microscopy, energy-dispersive X-ray spectroscopy, X-ray diffraction, UV−vis extinction spectroscopy, and thermal stability tests. The results demonstrate a highly stable semi-hollow gold-silver nanostar with LSPR maxima that can be tuned simply by adjusting the ratio of Ag:Au in the nanostar composition without the need to modify the nanostar dimensions.[25,37] Notably, the optical extinctions of the gold-silver nanostars span both ultraviolet and visible regions with an extended tail in the NIR region. Compared to gold nanostars, the bimetallic gold-silver nanostars also exhibited superior thermal and colloidal stability at elevated temperatures without the need for surface modification. Coupled with their enhanced stability, the ability to tune the extinction maxima of the new hAuAgNSts across UV-to-NIR wavelengths offers new opportunities in photocatalysis, biosensing, and other applications that utilize plasmonic nanostructures.

RESULTS AND DISCUSSION

Synthesis of Silver Nanostar Starting Materials. Colloidal silver nanostars were obtained using the method described in the experimental section. The scanning electron microscopy (SEM) and transmission electron microscopy (TEM) images in Figure 1a and Figure 1b, respectively, reveal that the synthesized silver nanostars have an average size of ∼190 nm with the number of arms varying from 8 to 16. A small number of overgrown silver nanostars exhibited secondary arms when the nanostar size is bigger than 300 nm. The size distribution of the silver nanostars was provided in the inset of Figure 1a.

Synthesis and Morphology of Semi-Hollow Gold-Silver Nanostars. As outlined in Scheme 1, the fabrication of semi-hollow gold-silver nanostars (hAuAgNSts) was achieved by galvanic replacement of silver nanostars in a basic gold salt (K-Au) solution containing potassium carbonate and hydrogen tetrachloroaurate hydrate. In the K-Au solution, metallic silver is oxidized by Au^{3+} ions to form Ag^{+} ions and metallic gold. During this process, silver atoms of AgNSts are replaced by gold atoms to form semi-hollow bimetallic gold-silver nanostars. The formation of the semi-hollow Au-Ag nanostars revealed characteristic pinhole features, as shown in Figure 1c and particularly Figure 1d. The pinhole features correspond to the sites of highly active galvanic replacement, which creates hollow cavities like those observed in previous studies involving the synthesis of hollow gold-silver nanoshells and other galvanically replaced bimetallic hollow nanostructures.[56−58] Due to the galvanic replacement process, the centers of the nanostar arms were often carved out, leaving the characteristic bright rim features in SEM images (Figure 1c) or dark rim features in TEM images (Figure 1d). Similar observations were also observed in other hollow metallic nanostructures.[56,59] More characteristic hollow features can be observed in the STEM images (*vide infra*). The size distribution of the Au-Ag nanostars is provided in the inset of Figure 1c. Interestingly, the etching process led to a shrinkage in size of the newly formed bimetallic hAuAgNSts; when compared to the starting Ag nanostars (∼190 nm), the average size of the gold-silver nanostars was found to be ∼170 nm.

The galvanic replacement process involved in the formation of the hAuAgNSts is illustrated in Scheme 2. When K-Au and

Scheme 2. Formation of Semi-Hollow Gold-Silver Nanostars via Galvanic Replacement on Silver Nanostars by Treatment with K-Gold Solution

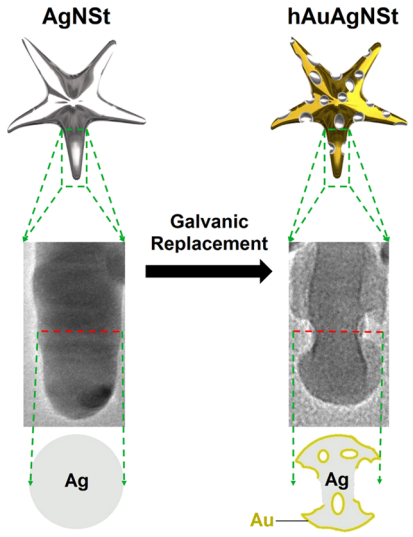

AgNSt colloidal solutions are mixed together, Ag atoms on the surface of the AgNSts are oxidized to form Ag^{+} ions in solution, while the Au atoms formed via the galvanic reduction of Au^{3+} ions are deposited on the surface of the Ag nanostar substrates.[56,57,60] The rapid oxidation taking place at the pinhole sites leads to rapid removal of silver atoms and the consequent generation of hollow cavities, as illustrated in Scheme 2.

In addition to the pinhole features, a greater number of depression areas can be observed on the surface of the semi-hollow gold-silver nanostars (see Figure 1d and Scheme 2) than the smoother surface of silver nanostars (Figure 1b). The widespread presence of the depression areas on the surface of the Au-Ag nanostars indicates that the galvanic corrosion and replacement of silver atoms by gold ions occurred at multiple sites across the nanostar structure. It should be noted that rapid and thorough mixing of the K-Au solution after adding to the AgNSt stock solution is critical to achieving a uniform population of hollow gold-silver nanostars. In particular, inadequately mixed solutions can give rise to severe corrosion of the silver nanostars to create "chopped-off" gold-silver pieces such as those shown in Figure S1.

Elemental Characterization of Semi-Hollow Gold-Silver Nanostars. We used energy-dispersive X-ray spectroscopy (EDX) to study the elemental composition and distribution of the semi-hollow gold-silver nanostars. Figure 2 shows a representative scanning transmission electron microscopy (STEM) image and the corresponding EDX elemental maps of the semi-hollow gold-silver nanostars prepared using our methodology. While Figure 2b confirms the presence of Ag atoms throughout the bimetallic nanostar, Figure 2c shows a uniform distribution of Au atoms throughout the bimetallic nanostar, which is consistent with the introduction of gold atoms via galvanic replacement. Additionally, the line-scan spectrum along one arm of a typical

https://doi.org/10.1021/acsanm.2c02462
ACS Appl. Nano Mater. 2022, 5, 11391−11399

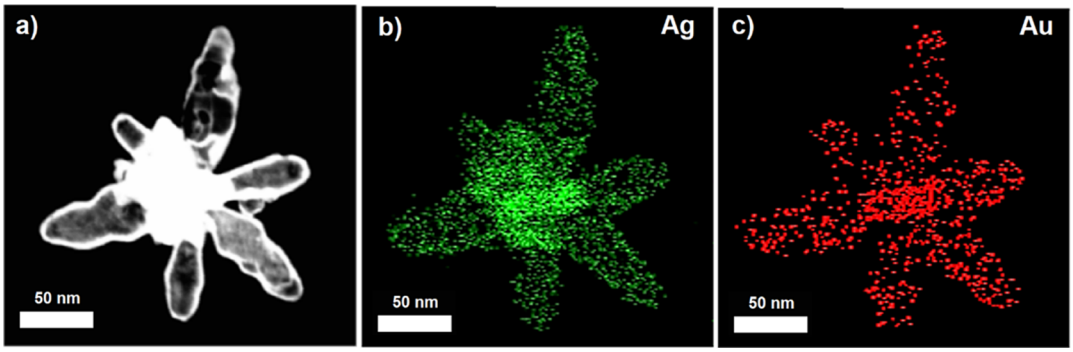

Figure 2. (a) STEM image and STEM-EDX elemental maps for (b) Ag and (c) Au in a typical semi-hollow gold-silver nanostar (hAuAgNSt).

semi-hollow gold-silver nanostar (Figure S2) also demonstrates the presence and uniform distribution of Ag and Au within the bimetallic gold-silver nanostar structure.

The EDX spectrum of the hollow gold-silver nanostars in the Supporting Information (Figure S3) confirms the presence of the characteristic Lα (2.98 keV) and Lβ (3.21 keV) peaks of silver as well as the characteristic Lα (9.71 keV) and Mα (2.13 keV) peaks of gold. A small Lα peak at 0.93 keV was also observed for the supporting copper grid of the TEM sample holder used in the measurement. Moreover, the atomic concentrations of gold in the bimetallic gold-silver nanostars formed in various etching conditions were also determined. The graph in Figure 3 shows the average Au atomic

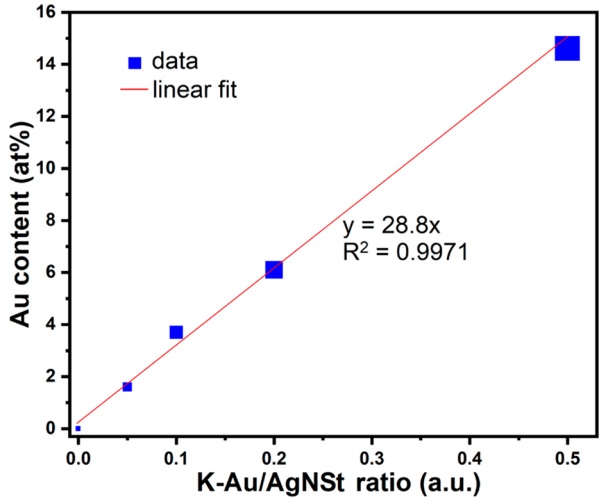

Figure 3. Au content of semi-hollow gold-silver nanostars synthesized using various ratios of K-Au and silver nanostar stock solutions. The size of the symbol reflects the error in the measured data point.

percentages in hAuAgNSts prepared with K-Au/AgNSt solution volume ratios of 0, 0.05, 0.1, 0.2, and 0.5. The linear relationship between the Au content in hAuAgNSts and the K-Au/AgNSt ratio allows for precise tunability of the elemental composition of the targeted bimetallic semi-hollow gold-silver nanostars. With the high R^2 value of the linear relation (>0.99), we anticipate that the trend toward longer LSPR wavelengths will continue with higher K-Au/AgNSt ratios such as 1 or more. This compositional flexibility is critical for fine-tuning the extinction maximum of the plasmon resonance of the hAuAgNSts and will be discussed in more detail in the Optical Properties section below.

Crystallinity of the Semi-Hollow Gold-Silver Nanostars. The crystalline characteristics of the three types of nanostars were evaluated using X-ray diffraction (XRD). Figure 4 shows the XRD patterns of hAuAgNSts, AuNSts, and

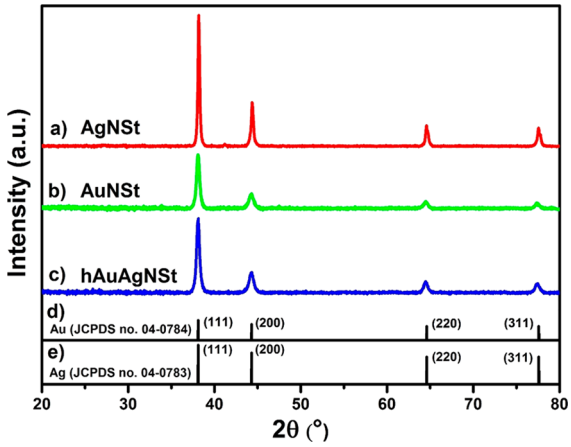

Figure 4. XRD spectra of (a) silver nanostars, (b) gold nanostars, and (c) semi-hollow gold-silver nanostars in comparison with the reference patterns of (d) gold and (e) silver.

AgNSts together with the reference peaks for pure Au (JCPDS card no. 04-0784) and pure Ag (JCPDS card no. 04-0783). For Ag nanostars (Figure 4a), strong diffraction peaks at 2θ = 38.15, 44.15, 64.42, and 77.34° corresponding to the respective (111), (200), (220), and (311) crystallographic planes of silver were observed. For Au nanostars (Figure 4b), strong peaks at 2θ = 38.21, 44.33, 64.72, and 77.74° corresponding to the respective (111), (200), (220), and (311) crystallographic planes of gold were observed. In the case of hollow gold-silver nanostars (Figure 4c), strong peaks at 2θ = 38.19, 44.23, 64.61, and 77.58° corresponding to the respective (111), (200), (220), and (311) crystallographic planes were observed. The comparable reflections and close proximity of the diffraction peaks from the three types of metallic nanostars can be attributed to the fact that both gold and silver have the same crystal structure (face-centered cubic) and possess similar atomic radii. Moreover, the average lattice constants of 408.29, 407.71, and 407.84 pm for AgNSts, AuNSts, and hAuAgNSts, respectively, were also calculated from the XRD patterns. Thus, the XRD results confirm the crystalline characteristics of metallic Au, Ag, and semi-hollow Au-Ag nanostars.

Optical Properties. UV−vis extinction spectra of the AgNSts, hAuAgNSts, and AuNSts were recorded and are presented in Figure 5; the corresponding localized surface

https://doi.org/10.1021/acsanm.2c02462
ACS Appl. Nano Mater. 2022, 5, 11391−11399

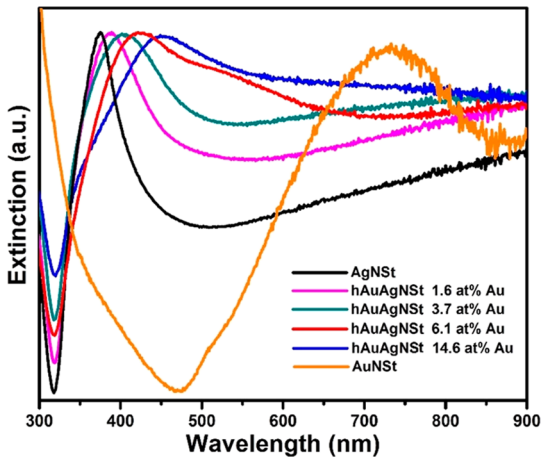

Figure 5. Extinction spectra of silver nanostars, semi-hollow gold-silver nanostars with varying Au content, and gold nanostars.

plasmon resonance (LSPR) maxima as a function of the Au content are provided in Table 1. The data show that with increasing atomic concentrations of gold, the extinction maxima shift from ~375 nm for the AgNSts to ~450 nm for the hAuAgNSts to ~730 nm for the AuNSts. Notably, at the highest concentrations of gold, the hAuAgNSts exhibit strong extinction tails that span the entire visible spectrum and parts of the near infrared. This broadband extinction characteristic makes the semi-hollow gold-silver nanostars potentially useful for radiation blocking.[61,62] Furthermore, the expansion from the UV region (5% of solar radiation)[55] into the visible (43% of solar radiation)[55] and NIR regions of the solar spectrum offers unique opportunities for a myriad of solar-driven applications that include photocatalysis,[29,30,48] photovoltaics,[31,32] and photothermal power generation.[63]

Similar to the phenomenon observed with plasmonic nanorods,[64] the broadening of the extinction peaks of hAuAgNSts with increased Au content can be attributed, at least in part, to the size shrinkage of the hAuAgNSts compared to the starting AgNSts (vide supra). Furthermore, it is likely that the extinction tail arises in part from the various longitudinal oscillation modes[65,66] along the many different arms of the gold-silver nanostars.[67] Perhaps more importantly, the broadening and redshifting of the extinction maxima can be attributed to the change in the Au-Ag nanostar composition[68] as well as the increased formation of hollow cavities when increasing the K-Au/AgNSt ratio in solution.[69] These relationships, when coupled with the previously discussed capacity to adjust the elemental composition of the hAuAgNSts, enable facile tuning of the optical responses of the semi-hollow gold-silver nanostars simply by adjusting the galvanic replacement conditions used in their preparation.

Stability Studies. Since the tendency of gold nanostars to aggregate leads to complications that often require surface functionalization[43−45] that limit the range of potential applications, we evaluated the thermal and colloidal stabilities of our unfunctionalized bimetallic gold-silver nanostars at elevated temperatures. As a first step, we determined the surface charges of AgNSts, hAuAgNSts, and AuNSts at room temperature using zeta potential measurements, which found that both AgNSts and hAuAgNSts have greater surface charges (−31.3 and −28.9 mV, respectively) than AuNSts (−25.5 mV); these measurements thus predict a higher colloidal stability for the new hAuAgNSts when compared to the more common AuNSts.

In further studies, Figure 6 shows the extinction spectra of the hollow gold-silver nanostars after heating for 1 h at 40, 60,

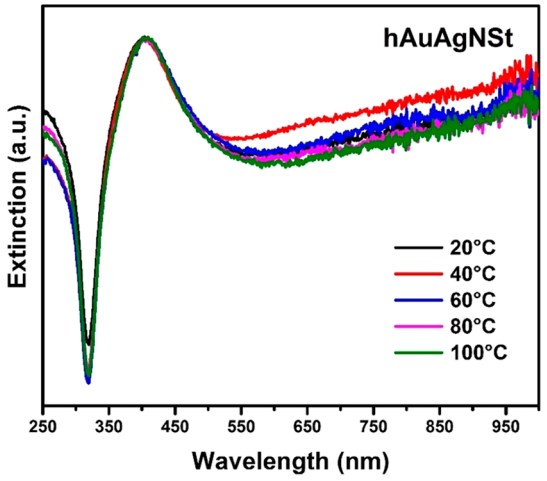

Figure 6. Extinction spectra of semi-hollow gold-silver nanostars (hAuAgNSts) after heating for 1 h at the indicated temperatures.

80, and 100 °C. Importantly, the spectra remained constant at all temperatures, indicating a high thermal and colloidal stability for the semi-hollow bimetallic Au-Ag nanostars. Notably, the size and morphology of the hAuAgNSts remained essentially unaffected after heating (Figure S5), which can be taken as a further indication of the stability of the hAuAgNSts.

Moreover, the hAuAgNSt solutions remained colloidally stable even after heating at 100 °C, as shown in Figure S6. In comparison, the AuNSt solution had visible aggregation even at room temperature (Figure S6). The optical response of AuNSts also varied significantly with temperature (Figure S7a and Table S1). The high stability even at elevated temperatures gives the newly developed bimetallic semi-hollow gold-silver nanostars significant potential for applications that require non-aggregated and/or non-functionalized nanostructures such as catalysis, photovoltaics, biosensing, and drug delivery. Furthermore, both hAuAgNSt and AgNSt as well as the Triton-stabilized AuNSt studied in this report still retained their optical and colloidal properties after at least 2 weeks of storage at 4 °C in the dark (i.e., conditions that we typically use for plasmonic nanoparticle storage).

Table 1. Localized Surface Plasmon Resonance Maxima and Au Content of Semi-Hollow Gold-Silver Nanostars at Various Ratios of K-Au/AgNSt

sample	AgNSt	hAuAgNSt	hAuAgNSt	hAuAgNSt	hAuAgNSt	AuNSt
K-Au/AgNSt	0	0.05	0.1	0.2	0.5	
Au at%	0	1.6 ± 0.2	3.7 ± 0.3	6.1 ± 0.3	14.6 ± 0.5	100
LSPR (nm)	~375	~390	~405	~425	~450	~730

https://doi.org/10.1021/acsanm.2c02462
ACS Appl. Nano Mater. 2022, 5, 11391−11399

CONCLUSIONS

This report demonstrates the fabrication of semi-hollow gold-silver nanostars (hAuAgNSts) via galvanic replacement of silver nanostars (AgNSts). The morphology, size distribution, surface charge, composition, crystallinity, and optical properties of the newly developed bimetallic Au-Ag nanostars were thoroughly characterized. Notably, the semi-hollow gold-silver nanostars exhibited enhanced thermal and colloidal stability when compared to conventional gold nanostars (AuNSts). Furthermore, simply by controlling the composition of the gold-silver nanostars, the optical extinctions of the hAuAgNSts were found to be tunable across ultraviolet and visible wavelengths with strong tailing into the near infrared. The versatile optical tunability, the broad and strong extinctions, and the enhanced thermal and colloidal stability render the hAuAgNSts potentially useful for a multitude of solar-driven applications such as photocatalysis, photovoltaics, radiation blocking, and biosensing.

MATERIALS AND METHODS

Materials. Silver nitrate (Sigma-Aldrich), trisodium citrate (EM Science), sodium hydroxide (Macron Chemicals), hydroxylamine (Thermo Fisher Scientific), hydrogen tetrachloroaurate(III) hydrate (Strem), potassium carbonate (J.T. Baker), nitric acid (EM Science), hydrochloric acid (EM Science), Triton X-100 (Sigma-Aldrich), sodium borohydride (Sigma-Aldrich), and ascorbic acid (Sigma-Aldrich) were purchased from the indicated suppliers and used without further purification. Deionized water was obtained from an Academic Milli-Q Water System (Millipore Corporation). All glassware used in the syntheses was cleaned with aqua regia solution ($HCl:HNO_3$ = 3:1), rinsed with Milli-Q water, and dried prior to use.

Synthesis of Silver Nanostars. Silver nanostars were prepared via modification of a previously reported method.[52] In a typical experiment, a mixture of 0.5 mL of 0.06 M hydroxylamine and 0.5 mL of 0.05 M NaOH was added into 9 mL of 0.111 mM $AgNO_3$ under magnetic stirring at 20 °C for 5 min in a 20 mL glass vial. Afterward, 100 μL of 0.03 M sodium citrate solution was added into the vial followed by 15 min of stirring. Shortly after the addition of sodium citrate, the color of the solution changed from transparent to murky gray, indicating the formation of silver nanostars. The final solution was then centrifuged at 8000 rpm for 15 min, and the volume reduced to 200 μL and kept as the AgNSt stock solution for further use.

Synthesis of Semi-Hollow Gold-Silver Nanostars. A potassium-containing gold salt solution (K-Au solution) was prepared by mixing 5 mL of 2 mM K_2CO_3 aqueous solution with 100 μL of 30 mM $HAuCl_4$ aqueous solution for 1 h. Semi-hollow gold-silver nanostars were fabricated via galvanic corrosion of the as-synthesized silver nanostars upon treatment with the K-Au solution. In typical experiments, 1 mL aliquots of AgNSt stock solution were placed in glass vials under vigorous stirring. Selected amounts of K-Au solution (0.05, 0.1, 0.2, and 0.5 mL) were injected into the vials containing the AgNSts followed by 5 h of stirring for the formation of hAuAgNSts possessing various amounts of gold. The final solutions were centrifuged at 8000 rpm for 15 min and then washed with deionized water three times before storage.

Synthesis of Gold Nanostars. Gold nanostars were synthesized via modification of a previously reported method.[70] Gold nanoseeds were prepared by adding 10 mL of 0.2 mM aqueous $HAuCl_4$ solution to 10 mL of 150 mM Triton X-100 aqueous solution; 600 μL of fresh cold 10 mM sodium borohydride was then added to the mixture to form the gold nanoseeds. Separately, the AuNSt growth solution was prepared by adding 280 μL of 4 mM $AgNO_3$ solution and 0.4 mL of 25 mM $HAuCl_4$ solution to 20 mL of a 150 mM aqueous solution of Triton X-100. Then, 300 μL of 0.78 M ascorbic acid solution was added to the growth solution at rt with stirring. When the mixture became colorless, 14 μL of the gold nanoseed solution was added to the growth solution. The solution turned blue and was stirred for another 8 h at rt to generate the gold nanostars.

Nanoparticle Characterization. All synthesized nanoparticles were imaged using a LEO-1525 scanning electron microscope (SEM) operating at 15 kV and 5.5 mm working distance. All SEM samples were deposited on pre-cleaned silicon wafers and dried at 60 °C in an oven for 1 h before imaging. An X'Pert powder X-ray diffractometer operating at 45 kV and 30 mA was used to assess the crystalline nature of the nanoparticles. All powder X-ray diffraction (PXRD) samples were prepared by drop-casting and drying on glass slides in an oven at 60 °C for 2 h. A JEOL JEM-2010 FX transmission electron microscope (TEM) with electron-dispersive X-ray spectroscopy (EDX) function operating at 200 kV was used to assess the morphology and the elemental distribution of the nanostars. All samples for TEM characterization were deposited on 300 mesh holey carbon-coated nickel grids and dried at 60 °C for 2 h before analysis. A Cary 50 scan UV−visible (UV−vis) spectrometer operating over a spectral range of 200−1000 nm was used to measure the optical properties of the synthesized nanostars. Zeta potential measurements were conducted on a Malvern Zetasizer model ZEN3600.

Stability Studies. The stabilities of the synthesized hAuAgNSts and AuNSts were assessed by heating their aqueous solutions at 20, 40, 60, 80, and 100 °C for 1 h followed by cooling to rt. At each temperature, the cooled-down nanostar solutions were checked for visible aggregation before having their extinction spectra recorded.

ASSOCIATED CONTENT

Supporting Information

The Supporting Information is available free of charge at https://pubs.acs.org/doi/10.1021/acsanm.2c02462.

SEM image of semi-hollow gold-silver nanostars (hAuAgNSts) with non-uniform mixing of K-Au and AgNSt stock solutions (Figure S1), TEM-EDX spectrum of hAuAgNSts (Figure S2), TEM-EDX elemental line scanning spectrum of hAuAgNSts (Figure S3), extinction spectra of silver nanoparticles, gold nanoparticles, and semi-hollow gold-silver nanostars (Figure S4), SEM images of hAuAgNSts at 20, 40, 60, 80, and 100 °C (Figure S5), images of gold, silver, and semi-hollow gold-silver nanostars in water after heating for 1 h at various temperatures (Figure S6), extinction spectra of gold, silver, and semi-hollow gold-silver nanostars after heating for 1 h at various temperatures (Figure S7), and LSPR peak positions of AuNSts and hAuAgNSts after heating for 1 h at various temperatures (Table S1) (PDF)

AUTHOR INFORMATION

Corresponding Author

T. Randall Lee − *Department of Chemistry and the Texas Center for Superconductivity, University of Houston, Houston, Texas 77204-5003, United States;* orcid.org/0000-0001-9584-8861; Email: trlee@uh.edu

Authors

Nhat M. Ngo − *Department of Chemistry and the Texas Center for Superconductivity, University of Houston, Houston, Texas 77204-5003, United States*

Mina Omidiyan − *Department of Chemistry and the Texas Center for Superconductivity, University of Houston, Houston, Texas 77204-5003, United States*

Hung-Vu Tran − *Department of Chemistry and the Texas Center for Superconductivity, University of Houston, Houston, Texas 77204-5003, United States;* orcid.org/0000-0001-8536-2737

https://doi.org/10.1021/acsanm.2c02462
ACS Appl. Nano Mater. 2022, 5, 11391−11399

Complete contact information is available at:
https://pubs.acs.org/10.1021/acsanm.2c02462

Notes

The authors declare no competing financial interest.

■ ACKNOWLEDGMENTS

The authors are grateful for the financial support from the Air Force Office of Scientific Research (AFOSR FA9550-20-1-0349), the Robert A. Welch Foundation (grant no. E-1320), and the Texas Center for Superconductivity at the University of Houston.

■ REFERENCES

(1) Baffou, G.; Cichos, F.; Quidant, R. Applications and Challenges of Thermoplasmonics. *Nat. Mater.* **2020**, *19*, 946−958.
(2) Yao, K.; Zhong, H.; Liu, Z.; Xiong, M.; Leng, S.; Zhang, J.; Xu, Y.; Wang, W.; Zhou, L.; Huang, H.; Jen, A. K.-Y. Plasmonic Metal Nanoparticles with Core−Bishell Structure for High-Performance Organic and Perovskite Solar Cells. *ACS Nano* **2019**, *13*, 5397−5409.
(3) Shi, X.; Ueno, K.; Oshikiri, T.; Sun, Q.; Sasaki, K.; Misawa, H. Enhanced Water Splitting under Modal Strong Coupling Conditions. *Nat. Nanotechnol.* **2018**, *13*, 953−958.
(4) Medhi, R.; Srinoi, P.; Ngo, N.; Tran, H.-V.; Lee, T. R. Nanoparticle-Based Strategies to Combat COVID-19. *ACS Appl. Nano Mater.* **2020**, *3*, 8557−8580.
(5) Zhang, Y.; Shuai, Z.; Zhou, H.; Luo, Z.; Liu, B.; Zhang, Y.; Zhang, L.; Chen, S.; Chao, J.; Weng, L.; Fan, Q.; Fan, C.; Huang, W.; Wang, L. Single-Molecule Analysis of Micro RNA and Logic Operations Using a Smart Plasmonic Nanobiosensor. *J. Am. Chem. Soc.* **2018**, *140*, 3988−3993.
(6) Hamans, R. F.; Parente, M.; Castellanos, G. W.; Ramezani, M.; Gómez Rivas, J.; Baldi, A. Super-Resolution Mapping of Enhanced Emission by Collective Plasmonic Resonances. *ACS Nano* **2019**, *13*, 4514−4521.
(7) Nugroho, F. A. A.; Darmadi, I.; Cusinato, L.; Susarrey-Arce, A.; Schreuders, H.; Bannenberg, L. J.; da Silva Fanta, A. B.; Kadkhodazadeh, S.; Wagner, J. B.; Antosiewicz, T. J.; Hellman, A.; Zhdanov, V. P.; Dam, B.; Langhammer, C. Metal−Polymer Hybrid Nanomaterials for Plasmonic Ultrafast Hydrogen Detection. *Nat. Mater.* **2019**, *18*, 489−495.
(8) Liu, T.; Zhang, Y.; Li, C.-H.; Marquez, M. D.; Tran, H.-V.; Robles Hernández, F. C.; Yao, Y.; Lee, T. R. Semihollow Core−Shell Nanoparticles with Porous SiO_2 Shells Encapsulating Elemental Sulfur for Lithium−Sulfur Batteries. *ACS Appl. Mater. Interfaces* **2020**, *12*, 47368−47376.
(9) Tran, H.-V.; Ngo, N. M.; Medhi, R.; Srinoi, P.; Liu, T.; Rittikulsittichai, S.; Lee, T. R. Multifunctional Iron Oxide Magnetic Nanoparticles for Biomedical Applications: A Review. *Materials* **2022**, *15*, 503.
(10) Schuller, J. A.; Barnard, E. S.; Cai, W.; Jun, Y. C.; White, J. S.; Brongersma, M. L. Plasmonics for Extreme Light Concentration and Manipulation. *Nat. Mater.* **2010**, *9*, 193−204.
(11) Linic, S.; Chavez, S.; Elias, R. Flow and Extraction of Energy and Charge Carriers in Hybrid Plasmonic Nanostructures. *Nat. Mater.* **2021**, *20*, 916−924.
(12) Tao, L.; Chen, K.; Chen, Z.; Cong, C.; Qiu, C.; Chen, J.; Wang, X.; Chen, H.; Yu, T.; Xie, W.; Deng, S.; Xu, J.-B. 1T′ Transition Metal Telluride Atomic Layers for Plasmon-Free SERS at Femtomolar Levels. *J. Am. Chem. Soc.* **2018**, *140*, 8696−8704.
(13) Meng, F.; Hao, W.; Yu, S.; Feng, R.; Liu, Y.; Yu, F.; Tao, P.; Shang, W.; Wu, J.; Song, C.; Deng, T. Vapor-Enabled Propulsion for Plasmonic Photothermal Motor at the Liquid/Air Interface. *J. Am. Chem. Soc.* **2017**, *139*, 12362−12365.
(14) Ng, C.; Cadusch, J. J.; Dligatch, S.; Roberts, A.; Davis, T. J.; Mulvaney, P.; Gómez, D. E. Hot Carrier Extraction with Plasmonic Broadband Absorbers. *ACS Nano* **2016**, *10*, 4704−4711.
(15) Collins, S. S. E.; Searles, E. K.; Tauzin, L. J.; Lou, M.; Bursi, L.; Liu, Y.; Song, J.; Flatebo, C.; Baiyasi, R.; Cai, Y.-Y.; Foerster, B.; Lian, T.; Nordlander, P.; Link, S.; Landes, C. F. Plasmon Energy Transfer in Hybrid Nanoantennas. *ACS Nano* **2021**, *15*, 9522−9530.
(16) Pettine, J.; Choo, P.; Medeghini, F.; Odom, T. W.; Nesbitt, D. J. Plasmonic Nanostar Photocathodes for Optically-Controlled Directional Currents. *Nat. Commun.* **2020**, *11*, 1367.
(17) Ou, Y.-C.; Wen, X.; Johnson, C. A.; Shae, D.; Ayala, O. D.; Webb, J. A.; Lin, E. C.; DeLapp, R. C.; Boyd, K. L.; Richmond, A.; Mahadevan-Jansen, A.; Rafat, M.; Wilson, J. T.; Balko, J. M.; Tantawy, M. N.; Vilgelm, A. E.; Bardhan, R. Multimodal Multiplexed Immunoimaging with Nanostars to Detect Multiple Immunomarkers and Monitor Response to Immunotherapies. *ACS Nano* **2020**, *14*, 651−663.
(18) Rotz, M. W.; Culver, K. S. B.; Parigi, G.; MacRenaris, K. W.; Luchinat, C.; Odom, T. W.; Meade, T. J. High Relaxivity Gd (III)−DNA Gold Nanostars: Investigation of Shape Effects on Proton Relaxation. *ACS Nano* **2015**, *9*, 3385−3396.
(19) Gao, Y.; Wang, J.; Wang, W.; Zhao, T.; Cui, Y.; Liu, P.; Xu, S.; Luo, X. More Symmetrical "Hot Spots" Ensure Stronger Plasmon-Enhanced Fluorescence: From Au Nanorods to Nanostars. *Anal. Chem.* **2021**, *93*, 2480−2489.
(20) Ngo, N. M.; Tran, H.-V.; Lee, T. R. Plasmonic Nanostars: A Systematic Review of Their Synthesis and Applications. *ACS Appl. Nano Mater.(submitted)*
(21) Ning, S.; Zhang, N.; Dong, H.; Hou, X.; Zhang, F.; Wu, Z. Enhanced Lasing from Organic Gain Medium by Au Nanocube@SiO_2 Core-Shell Nanoparticles with Optimal Size. *Opt. Mater. Express* **2018**, *8*, 3014.
(22) Gutiérrez, Y.; Alcaraz de la Osa, R.; Ortiz, D.; Saiz, J. M.; González, F.; Moreno, F. Plasmonics in the Ultraviolet with Aluminum, Gallium, Magnesium and Rhodium. *Appl. Sci.* **2018**, *8*, 64.
(23) Nagy, B. J.; Pápa, Z.; Péter, L.; Prietl, C.; Krenn, J. R.; Dombi, P. Near-Field-Induced Femtosecond Breakdown of Plasmonic Nanoparticles. *Plasmonics* **2020**, *15*, 335−340.
(24) Zhuang, C.; Xu, Y.; Xu, N.; Wen, J.; Chen, H.; Deng, S. Plasmonic Sensing Characteristics of Gold Nanorods with Large Aspect Ratios. *Sensors* **2018**, *18*, 3458.
(25) Dacarro, G.; Pallavicini, P.; Bertani, S. M.; Chirico, G.; D'Alfonso, L.; Falqui, A.; Marchesi, N.; Pascale, A.; Sironi, L.; Taglietti, A.; Zuddas, E. Synthesis of Reduced-Size Gold Nanostars and Internalization in SH-SY5Y Cells. *J. Colloid Interface Sci.* **2017**, *505*, 1055−1064.
(26) Barbosa, S.; Agrawal, A.; Rodríguez-Lorenzo, L.; Pastoriza-Santos, I.; Alvarez-Puebla, R. A.; Kornowski, A.; Weller, H.; Liz-Marzán, L. M. Tuning Size and Sensing Properties in Colloidal Gold Nanostars. *Langmuir* **2010**, *26*, 14943−14950.
(27) Zhang, S.; Geryak, R.; Geldmeier, J.; Kim, S.; Tsukruk, V. V. Synthesis, Assembly, and Applications of Hybrid Nanostructures for Biosensing. *Chem. Rev.* **2017**, *117*, 12942−13038.
(28) Dondapati, S. K.; Sau, T. K.; Hrelescu, C.; Klar, T. A.; Stefani, F. D.; Feldmann, J. Label-Free Biosensing Based on Single Gold Nanostars as Plasmonic Transducers. *ACS Nano* **2010**, *4*, 6318−6322.
(29) de Barros, H. R.; García, I.; Kuttner, C.; Zeballos, N.; Camargo, P. H. C.; de Torresi, S. I. C.; López-Gallego, F.; Liz-Marzán, L. M. Mechanistic Insights into the Light-Driven Catalysis of an Immobilized Lipase on Plasmonic Nanomaterials. *ACS Catal.* **2021**, *11*, 414−423.
(30) Kumar, D.; Lee, S. B.; Park, C. H.; Kim, C. S. Impact of Ultrasmall Platinum Nanoparticle Coating on Different Morphologies of Gold Nanostructures for Multiple One-Pot Photocatalytic Environment Protection Reactions. *ACS Appl. Mater. Interfaces* **2018**, *10*, 389−399.
(31) Ginting, R. T.; Kaur, S.; Lim, D.-K.; Kim, J.-M.; Lee, J. H.; Lee, S. H.; Kang, J.-W. Plasmonic Effect of Gold Nanostars in Highly Efficient Organic and Perovskite Solar Cells. *ACS Appl. Mater. Interfaces* **2017**, *9*, 36111−36118.
(32) Batmunkh, M.; Macdonald, T. J.; Peveler, W. J.; Bati, A. S. R.; Carmalt, C. J.; Parkin, I. P.; Shapter, J. G. Plasmonic Gold Nanostars

Incorporated into High-Efficiency Perovskite Solar Cells. *Chem SusChem* **2017**, *10*, 3750−3753.
(33) Gopalakrishnan, A.; Chirumamilla, M.; De Angelis, F.; Toma, A.; Zaccaria, R. P.; Krahne, R. Bimetallic 3D Nanostar Dimers in Ring Cavities: Recyclable and Robust Surface-Enhanced Raman Scattering Substrates for Signal Detection from Few Molecules. *ACS Nano* **2014**, *8*, 7986−7994.
(34) Zhang, W.; Liu, J.; Niu, W.; Yan, H.; Lu, X.; Liu, B. Tip-Selective Growth of Silver on Gold Nanostars for Surface-Enhanced Raman Scattering. *ACS Appl. Mater. Interfaces* **2018**, *10*, 14850−14856.
(35) Han, X.; Xu, Y.; Li, Y.; Zhao, X.; Zhang, Y.; Min, H.; Qi, Y.; Anderson, G. J.; You, L.; Zhao, Y.; Nie, G. An Extendable Star-Like Nanoplatform for Functional and Anatomical Imaging-Guided Photothermal Oncotherapy. *ACS Nano* **2019**, *13*, 4379−4391.
(36) Cai, Z.; Zhang, Y.; He, Z.; Jiang, L.-P.; Zhu, J.-J. NIR-Triggered Chemo-Photothermal Therapy by Thermosensitive Gold Nanostar@Mesoporous Silica@Liposome-Composited Drug Delivery Systems. *ACS Appl. Bio Mater.* **2020**, *3*, 5322−5330.
(37) de Puig, H.; Tam, J. O.; Yen, C.-W.; Gehrke, L.; Hamad-Schifferli, K. Extinction Coefficient of Gold Nanostars. *J. Phys. Chem. C* **2015**, *119*, 17408−17415.
(38) Ma, J.; Liu, X.; Wang, R.; Zhang, J.; Jiang, P.; Wang, Y.; Tu, G. Bimetallic Core−Shell Nanostars with Tunable Surface Plasmon Resonance for Surface-Enhanced Raman Scattering. *ACS Appl. Nano Mater.* **2020**, *3*, 10885−10894.
(39) Theodorou, I. G.; Jawad, Z. A. R.; Jiang, Q.; Aboagye, E. O.; Porter, A. E.; Ryan, M. P.; Xie, F. Gold Nanostar Substrates for Metal-Enhanced Fluorescence through the First and Second Near-Infrared Windows. *Chem. Mater.* **2017**, *29*, 6916−6926.
(40) Xi, W.; Phan, H. T.; Haes, A. J. How to Accurately Predict Solution-Phase Gold Nanostar Stability. *Anal. Bioanal. Chem.* **2018**, *410*, 6113−6123.
(41) Pamies, R.; Cifre, J. G. H.; Espín, V. F.; Collado-González, M.; Baños, F. G. D.; de la Torre, J. G. Aggregation Behaviour of Gold Nanoparticles in Saline Aqueous Media. *J. Nanopart. Res.* **2014**, *16*, 2376.
(42) Li, Y.; Wu, P.; Xu, H.; Zhang, H.; Zhong, X. Anti-Aggregation of Gold Nanoparticle-Based Colorimetric Sensor for Glutathione with Excellent Selectivity and Sensitivity. *The Analyst* **2011**, *136*, 196−200.
(43) Tian, Y.; Zhang, Y.; Teng, Z.; Tian, W.; Luo, S.; Kong, X.; Su, X.; Tang, Y.; Wang, S.; Lu, G. pH-Dependent Transmembrane Activity of Peptide-Functionalized Gold Nanostars for Computed Tomography/Photoacoustic Imaging and Photothermal Therapy. *ACS Appl. Mater. Interfaces* **2017**, *9*, 2114−2122.
(44) Yin, T.; Xie, W.; Sun, J.; Yang, L.; Liu, J. Penetratin Peptide-Functionalized Gold Nanostars: Enhanced BBB Permeability and NIR Photothermal Treatment of Alzheimer's Disease Using Ultralow Irradiance. *ACS Appl. Mater. Interfaces* **2016**, *8*, 19291−19302.
(45) Ki, J.; Jang, E.; Han, S.; Shin, M.-K.; Kang, B.; Huh, Y.-M.; Haam, S. Instantaneous pH-Boosted Functionalization of Stellate Gold Nanoparticles for Intracellular Imaging of MiRNA. *ACS Appl. Mater. Interfaces* **2017**, *9*, 17702−17709.
(46) Ma, T.; Yang, W.; Liu, S.; Zhang, H.; Liang, F. A Comparison Reduction of 4-Nitrophenol by Gold Nanospheres and Gold Nanostars. *Catalysts* **2017**, *7*, 38.
(47) Zhu, S.-Q.; Bian, B.; Zhu, Y.-F.; Yang, J.; Zhang, D.; Feng, L. Enhancement in Power Conversion Efficiency of GaAs Solar Cells by Utilizing Gold Nanostar Film for Light-Trapping. *Front. Chem.* **2019**, *7*, 137.
(48) Li, C.-H.; Li, M.-C.; Liu, S.-P.; Jamison, A. C.; Lee, D.; Lee, T. R.; Lee, T.-C. Plasmonically Enhanced Photocatalytic Hydrogen Production from Water: The Critical Role of Tunable Surface Plasmon Resonance from Gold−Silver Nanoshells. *ACS Appl. Mater. Interfaces* **2016**, *8*, 9152−9161.
(49) Oliveira, M. J.; Quaresma, P.; Peixoto de Almeida, M.; Araújo, A.; Pereira, E.; Fortunato, E.; Martins, R.; Franco, R.; Águas, H. Office Paper Decorated with Silver Nanostars - an Alternative Cost Effective Platform for Trace Analyte Detection by SERS. *Sci. Rep.* **2017**, *7*, 2480.
(50) Verma, A. K.; Soni, R. K. Multi-Spiked Silver Stars for Ultrasensitive and Multiplexed SERS Detection of Analytes. *J. Phys. D: Appl. Phys.* **2021**, *54*, 475107.
(51) Zalaffi, M. S.; Litti, L.; Canton, P.; Meneghetti, M.; Moretto, L. M.; Ugo, P. Preparation and Characterization of Ag-Nanostars@Au-Nanowires Hierarchical Nanostructures for Highly Sensitive Surface Enhanced Raman Spectroscopy. *Nano Express* **2020**, *1*, No. 020006.
(52) Garcia-Leis, A.; Garcia-Ramos, J. V.; Sanchez-Cortes, S. Silver Nanostars with High SERS Performance. *J. Phys. Chem. C* **2013**, *117*, 7791−7795.
(53) Bessa, L. J.; Peixoto de Almeida, M.; Eaton, P.; Pereira, E.; Gameiro, P. Silver Nanostars-Coated Surfaces with Potent Biocidal Properties. *Int. J. Environ. Res. Public Health* **2020**, *17*, 7891.
(54) Garcia-Leis, A.; Rivera-Arreba, I.; Sanchez-Cortes, S. Morphological Tuning of Plasmonic Silver Nanostars by Controlling the Nanoparticle Growth Mechanism: Application in the SERS Detection of the Amyloid Marker Congo Red. *Colloids Surf., A* **2017**, *535*, 49−60.
(55) Kruse, O.; Rupprecht, J.; Mussgnug, J. H.; Dismukes, G. C.; Hankamer, B. Photosynthesis: A Blueprint for Solar Energy Capture and Biohydrogen Production Technologies. *Photochem. Photobiol. Sci.* **2005**, *4*, 957.
(56) Vongsavat, V.; Vittur, B. M.; Bryan, W. W.; Kim, J.-H.; Lee, T. R. Ultrasmall Hollow Gold−Silver Nanoshells with Extinctions Strongly Red-Shifted to the Near-Infrared. *ACS Appl. Mater. Interfaces* **2011**, *3*, 3616−3624.
(57) Tan, S. F.; Lin, G.; Bosman, M.; Mirsaidov, U.; Nijhuis, C. A. Real-Time Dynamics of Galvanic Replacement Reactions of Silver Nanocubes and Au Studied by Liquid-Cell Transmission Electron Microscopy. *ACS Nano* **2016**, *10*, 7689−7695.
(58) Kang, Y. S.; Jung, J. Y.; Choi, D.; Sohn, Y.; Lee, S.-H.; Lee, K.-S.; Kim, N. D.; Kim, P.; Yoo, S. J. Formation Mechanism and Gram-Scale Production of PtNi Hollow Nanoparticles for Oxygen Electrocatalysis through In Situ Galvanic Displacement Reaction. *ACS Appl. Mater. Interfaces* **2020**, *12*, 16286−16297.
(59) Zhang, L.; Chen, P.; Loiseau, A.; Brouri, D.; Casale, S.; Salmain, M.; Boujday, S.; Liedberg, B. Spatially Controlled Reduction and Growth of Silver in Hollow Gold Nanoshell Particles. *J. Phys. Chem. C* **2019**, *123*, 10614−10621.
(60) Goris, B.; Polavarapu, L.; Bals, S.; Van Tendeloo, G.; Liz-Marzán, L. M. Monitoring Galvanic Replacement Through Three-Dimensional Morphological and Chemical Mapping. *Nano Lett.* **2014**, *14*, 3220−3226.
(61) Besteiro, L. V.; Kong, X.-T.; Wang, Z.; Rosei, F.; Govorov, A. O. Plasmonic Glasses and Films Based on Alternative Inexpensive Materials for Blocking Infrared Radiation. *Nano Lett.* **2018**, *18*, 3147−3156.
(62) Kunz, J. N.; Voronine, D. V.; Lu, W.; Liege, Z.; Lee, H. W. H.; Zhang, Z.; Scully, M. O. Aluminum Plasmonic Nanoshielding in Ultraviolet Inactivation of Bacteria. *Sci. Rep.* **2017**, *7*, 9026.
(63) Kashyap, V.; Sakunkaewkasem, S.; Jafari, P.; Nazari, M.; Eslami, B.; Nazifi, S.; Irajizad, P.; Marquez, M. D.; Lee, T. R.; Ghasemi, H. Full Spectrum Solar Thermal Energy Harvesting and Storage by a Molecular and Phase-Change Hybrid Material. *Joule* **2019**, *3*, 3100−3111.
(64) Juvé, V.; Cardinal, M. F.; Lombardi, A.; Crut, A.; Maioli, P.; Pérez-Juste, J.; Liz-Marzán, L. M.; Del Fatti, N.; Vallée, F. Size-Dependent Surface Plasmon Resonance Broadening in Nonspherical Nanoparticles: Single Gold Nanorods. *Nano Lett.* **2013**, *13*, 2234−2240.
(65) Sahu, A. K.; Das, A.; Ghosh, A.; Raj, S. Understanding Blue Shift of the Longitudinal Surface Plasmon Resonance during Growth of Gold Nanorods. *Nano Express* **2021**, *2*, No. 010009.
(66) Chen, F.; Alemu, N.; Johnston, R. L. Collective Plasmon Modes in a Compositionally Asymmetric Nanoparticle Dimer. *AIP Adv.* **2011**, *1*, No. 032134.

https://doi.org/10.1021/acsanm.2c02462
ACS Appl. Nano Mater. 2022, 5, 11391−11399

(67) Ziegler, J.; Wörister, C.; Vidal, C.; Hrelescu, C.; Klar, T. A. Plasmonic Nanostars as Efficient Broadband Scatterers for Random Lasing. *ACS Photonics* **2016**, *3*, 919−923.
(68) Motl, N. E.; Ewusi-Annan, E.; Sines, I. T.; Jensen, L.; Schaak, R. E. Au−Cu Alloy Nanoparticles with Tunable Compositions and Plasmonic Properties: Experimental Determination of Composition and Correlation with Theory. *J. Phys. Chem. C* **2010**, *114*, 19263−19269.
(69) Genç, A.; Patarroyo, J.; Sancho-Parramon, J.; Bastús, N. G.; Puntes, V.; Arbiol, J. Hollow Metal Nanostructures for Enhanced Plasmonics: Synthesis, Local Plasmonic Properties and Applications. *Nanophotonics* **2017**, *6*, 193−213.
(70) Atta, S.; Beetz, M.; Fabris, L. Understanding the Role of $AgNO_3$ Concentration and Seed Morphology in the Achievement of Tunable Shape Control in Gold Nanostars. *Nanoscale* **2019**, *11*, 2946−2958.

https://doi.org/10.1021/acsanm.2c02462
ACS Appl. Nano Mater. 2022, 5, 11391−11399